Strain pre-extrapolation methods for shape sensing: A comparative study between modal virtual sensor expansion and smoothing element analysis

Results in Engineering 29 (2026) 109109

Contents lists available at ScienceDirect

Results in Engineering

journal homepage: www.sciencedirect.com/journal/results-in-engineering

Research paper

Strain pre-extrapolation methods for shape sensing: A comparative study between modal virtual sensor expansion and smoothing element analysis

Marco Esposito

Department of Mechanical and Aerospace Engineering, Politecnico di Torino, Corso Duca degli Abruzzi, 24, 10129, Torino, Italy

ARTICLE INFO

Keywords:
Structural Health Monitoring
iFEM
Modal VSE
SEA
Shape sensing
Strain pre-extrapolation

ABSTRACT

Reconstructing displacement fields from sparse strain measurements, commonly referred to as shape sensing, has become a key component in developing effective Structural Health Monitoring (SHM) systems and for enabling accurate digital twin representations of engineering structures. Among available techniques, the inverse Finite Element Method (iFEM) is widely used but typically requires a dense sensor network. To reduce this dependency, strain pre-extrapolation methods are employed. The most established approach is Smoothing Element Analysis (SEA), which performs well for simple geometries but struggles with complex built-up structures. A recently proposed alternative, the Modal Virtual Sensor Expansion (Modal VSE), leverages modal strain shapes to virtually expand the strain field and has shown promising results, though it has not yet been benchmarked against existing methods. This study provides the first direct comparison between Modal VSE and SEA for strain pre-extrapolation and subsequent iFEM-based shape sensing of a composite stiffened panel. Results demonstrate that Modal VSE achieves higher accuracy and better adaptability across the examined configurations. Its superior performance persists even when sensor signals are corrupted by noise representative of experimental conditions. These findings highlight Modal VSE as a robust and effective tool for enhancing shape sensing in complex structural domains, thereby supporting more practical implementations of iFEM-based SHM and digital twin frameworks.

1. Introduction

Shape sensing refers to the process of reconstructing the deformed shape of a structure using discrete strain measurements. This technique is increasingly gaining significance for the development of modern Structural Health Monitoring (SHM) frameworks. Continuous monitoring of displacements throughout a structure's service life can provide essential information regarding its health, enabling the detection of damage and facilitating efficient maintenance strategies [1–8]. Moreover, shape sensing can also serve as a feedback monitoring system for controlling the morphing mechanisms in newly developed smart structures [9–11].

Several shape sensing methods have been proposed over the past two decades. Recent progress in strain-sensing technology [12,13] has driven the development of advanced strain-based algorithms. While all these methods aim to compute the displacement field from discrete strain measurements, they differ in their underlying principles [14]. This work focuses on the inverse Finite Element Method (iFEM), which has gained significant recognition in the open literature for its effectiveness and versatility. The success of the method stems from its superior accuracy compared to other existing approaches [15,16], its independence from material property knowledge, and its applicability to both thin-walled shell geometries and beam-like structures, unlike alternative techniques that are restricted to the latter [17,18]. iFEM, originally introduced in [19], relies on discretising the structural domain using finite elements and approximating the strain field in terms of nodal degrees of freedom (displacements and rotations) and shape functions. The discrepancy between this analytical strain field and the measured strains at selected locations is minimised to determine the nodal values of the degrees of freedom that best fit the experimental data. The iFEM has been successfully applied to beam-like structures [20–22], thin-walled structures [14,23], as well as sandwich and multilayered composite structures [24–27]. Recent developments have extended the method's modelling capabilities through isogeometric formulations [28,29]. Furthermore, in [30], iFEM has been adapted for damage detection via the reconstruction of the modal parameters of plate structures. Damage identification in multilayered plates has also been addressed in [31] through the integration of Refined Zigzag Theory (RZT) into the iFEM framework. In several applications and comparative studies [14–16], iFEM has proven to be more accurate than other shape sensing methods. The impressive accuracy of the method comes at a cost; the method requires a significant number of strain sensors to deliver its best performance. This limitation reduces the applicability of the method to real structures, where the availability of strain sensors is often limited. A step

E-mail address: marco.esposito@polito.it

https://doi.org/10.1016/j.rineng.2026.109109
Received 21 May 2025; Received in revised form 12 January 2026; Accepted 12 January 2026
Available online 15 January 2026

forward in overcoming this limitation has been recently proposed in Biscotti et al. [32], where the Single Sensor Based iFEM (SSB-iFEM) has been formulated. This formulation removes the standard iFEM requirement for back-to-back sensors, allowing the sensorisation of thin-walled structures with single-sided sensor configurations and thus reducing the sensor requirement for the method. This formulation has been successfully applied to the monitoring of a container ship in Bardiani et al. [33].

Another strategy to reduce the strain sensor requirement for iFEM is the use of strain pre-extrapolation techniques. In Wang et al. [34], the full strain field of a CFRP plate is reconstructed from a limited number of strain measurements through a moving-surface spline interpolation based on Green's functions. Despite this promising approach, the challenge of enriching iFEM input with additional strain data from a limited number of physical sensors installed has been addressed in only a few studies. One of the first approaches was the Smoothing Element Analysis (SEA), introduced in [35] as a finite element-based method for extrapolating individual stress components across a domain with adjustable smoothness. SEA was later adapted to handle strain components and integrated with iFEM for applications such as experimental shape sensing of a wing-shaped sandwich laminate [36] and, more recently, numerical shape reconstruction of an aluminium plate [37]. In [38], SEA has been coupled with a sensor optimisation algorithm to increase the efficiency of the method and further reduce the number of sensors required by iFEM. An alternative strategy based on polynomial fitting was proposed in [39] for the same purpose. A comparative assessment of SEA and polynomial fitting was conducted in [40], focusing on an experimental case involving a composite plate under buckling conditions and showing the superior extrapolation capabilities of SEA. Although SEA is widely adopted as the standard technique for extrapolating strain data for iFEM, its applicability is generally limited to simple geometries. Specifically, it can only propagate strain information within regions lying on the same continuous surface as the sensor data, i.e. strains recorded on the skin of a stiffened panel cannot be used to infer strains on the stiffeners, and vice versa. Additionally, since this technique operates on scalar quantities, each strain component must be extrapolated separately, resulting in complex processes. A new strain pre-extrapolation technique, the Modal Virtual Sensor Expansion (Modal VSE), has been recently formulated and coupled with iFEM in [41]. This method is inspired by an established shape sensing technique, renowned for its adaptability to sparse strain sensor configurations, the Modal Method (MM) [42]. The Modal VSE employs modal strain shapes as basis functions to reconstruct the full strain field of a structure. The coefficients of the basis functions are determined by fitting the modal strain expansion to discrete strain measurements, in a least-squares sense, using data from a limited number of sensors. This technique overcomes the limitations of SEA in terms of its applicability to complex geometries. In fact, since the modal strain shapes are defined across the entire structural domain and account for all strain components in every direction, the virtual expansion is not limited by the location or direction of the input data. For instance, starting from discrete strain components measured along the x-direction on one surface of a structure, it is possible to compute strain components in the y-direction on a different surface of the same structure. The novelty introduced by the Modal VSE has demonstrated promising results; however, it has never been compared with other strain pre-extrapolation models. A rigorous comparative study assessing the performance of the Modal VSE is therefore highly needed, both for researchers and industrial practitioners, to determine the most suitable tool for their specific applications.

In this work, the Modal VSE method is benchmarked against the most widely used pre-extrapolation approach, SEA. The comparative study is numerically performed on the extrapolation of strains of a composite wing-shaped panel. Starting from a reduced set of sensors, the two methods are used to expand the strain information and feed the iFEM for shape sensing. The analysis also includes an uncertainty propagation analysis, performed through a Monte Carlo Simulation process [16], to evaluate the influence of errors that may affect the inputs from experimentally measured strains. The study shows that the Modal VSE is more adaptable to complex geometries and consistently more accurate than SEA for strain pre-extrapolation. Moreover, although iFEM demonstrates strong robustness and is only slightly affected by variations in the strain input, the use of Modal VSE for strain pre-extrapolation also leads to improved accuracy in shape sensing. These conclusions are also confirmed in the uncertainty propagation study, when the input strains are affected by errors simulating experimental scenarios.

The paper is structured as follows. In Section 2, iFEM is introduced. The strain pre-extrapolation methods, the Modal VSE and SEA, are described in detail in Section 3. In Section 4, the test case and the results of the strain pre-extrapolation and shape sensing are presented. The effects of the uncertainty in the strain input are evaluated in Section 5. Finally, in Section 6, the concluding remarks are formulated.

2. Inverse Finite Element Method

The inverse Finite Element Method (iFEM) is founded on the discretisation of the structural domain into finite elements. Similar to the conventional (direct) Finite Element Method, the displacement field within each element is interpolated through unknown nodal degrees of freedom (DOFs) and predefined spatial shape functions [43]. This formulation enables the direct derivation of the strain field from the spatial derivatives of the shape functions and the nodal degrees of freedom [44].

Adopting the First-order Shear Deformation Theory as the kinematic assumption for thin plates, the strain field, which includes three in-plane strain components and two transverse shear strain components, can be represented in terms of eight strain measures, $\varepsilon_k\,(k = 1,\ 2,\ \ldots,\ 8)$:

$$\begin{Bmatrix}\varepsilon_{xx}\\ \varepsilon_{yy}\\ \gamma_{xy}\end{Bmatrix} = \begin{Bmatrix}u_{,x}\\ v_{,y}\\ v_{,x}+u_{,y}\end{Bmatrix} + z\begin{Bmatrix}\theta_{y,x}\\ -\theta_{x,y}\\ (\theta_{y,y}-\theta_{x,x})\end{Bmatrix} = \begin{Bmatrix}\varepsilon_1\\ \varepsilon_2\\ \varepsilon_3\end{Bmatrix} + z\begin{Bmatrix}\varepsilon_4\\ \varepsilon_5\\ \varepsilon_6\end{Bmatrix} = \boldsymbol{e} + z\boldsymbol{k}$$
$$\begin{Bmatrix}\gamma_{xz}\\ \gamma_{yz}\end{Bmatrix} = \begin{Bmatrix}w_{,x}+\theta_y\\ w_{,y}-\theta_x\end{Bmatrix} = \begin{Bmatrix}\varepsilon_7\\ \varepsilon_8\end{Bmatrix} = \boldsymbol{g} \tag{1}$$

in the above, $\boldsymbol{e}$ denotes the membrane strain measures, $\boldsymbol{k}$ the bending curvatures, and $\boldsymbol{g}$ the transverse shear strain measures. The mid-plane displacements and the bending rotations are u, v, w, θ_x, and θ_y, and z is the through-thickness coordinate.

By discretising the structure with finite elements, these kinematic variables within each element can be interpolated through the shape function matrix $\mathbf{N}$ and the vector of nodal degrees of freedom $\mathbf{u}^e$:

$$[u,\ v,\ w,\ \theta_x,\ \theta_y]^T = \mathbf{N}\mathbf{u}^e \tag{2}$$

The eight strain measures defined in Eq. (1) are thus expressed in terms of the nodal degrees of freedom as:

$$\varepsilon_k(\mathbf{u}^e) = \mathbf{B}_k\mathbf{u}^e \quad (k = 1,\ 2,\ \ldots,\ 8) \tag{3}$$

here, $\mathbf{B}_k$ is a matrix containing the spatial derivatives of the shape functions corresponding to the kth strain measure.

The aim of iFEM is to determine the nodal degrees of freedom that optimally match, in a least-squares sense, the analytical strain measures (Eq. (3)) to experimentally obtained strains at discrete locations. This is accomplished by minimising the following functional:

$$\Psi^e(\mathbf{u}^e) = \sum_{k=1}^{8}\lambda_k^e w_k^e \iint_{A^e}(\varepsilon_k(\mathbf{u}^e) - \varepsilon_k^m)^2 dx dy \tag{4}$$

in this expression, ε_k^m represents the kth strain measure obtained experimentally, and A^e denotes the area of the inverse element. The coefficients w_k^e ensure dimensional consistency across terms and are set as $w_k^e = 1$ for $k = 1, 2, 3, 7, 8$, and $w_k^e = (2h)^2$ for $k = 4, 5, 6$, with h being the half-thickness of the plate. The coefficients λ_k^e are penalisation factors which reflect whether the kth strain measure is available or not: they are set to 1 if the strain is measured, and to a small value (e.g., $10^{-4}, 10^{-5}, 10^{-6}$) otherwise. In the latter case, ε_k^m is assumed to be zero.

The first six strain measures can be experimentally estimated at a generic location (g) by using data from sensors placed on both the top (+) and bottom (-) surfaces of a plate:

$$\mathbf{e}^m_{(g)} = \begin{Bmatrix} \varepsilon^m_1 \\ \varepsilon^m_2 \\ \varepsilon^m_3 \end{Bmatrix}_{(g)} = \frac{1}{2}\begin{Bmatrix} \varepsilon^+_{xx} + \varepsilon^-_{xx} \\ \varepsilon^+_{yy} + \varepsilon^-_{yy} \\ \gamma^+_{xy} + \gamma^-_{xy} \end{Bmatrix}_{(g)} \tag{5a}$$

$$\mathbf{k}^m_{(g)} = \begin{Bmatrix} \varepsilon^m_4 \\ \varepsilon^m_5 \\ \varepsilon^m_6 \end{Bmatrix}_{(g)} = \frac{1}{2h}\begin{Bmatrix} \varepsilon^+_{xx} - \varepsilon^-_{xx} \\ \varepsilon^+_{yy} - \varepsilon^-_{yy} \\ \gamma^+_{xy} - \gamma^-_{xy} \end{Bmatrix}_{(g)} \tag{5b}$$

If only unidirectional sensors are used, only certain strain components can be reconstructed; the remaining components are addressed via the penalisation scheme using λ^e_k. The transverse shear strain measures, ε_7 and ε_8 (see Eq. (1)), cannot be experimentally measured and are always associated with small penalty values $\lambda^e_{7,8}$ and zero measured values $\varepsilon^m_{7,8}$.

Minimising the functional in Eq. (4) yields the nodal degrees of freedom that best fit the measured strain field in a least-squares sense. This minimisation leads to a system of linear algebraic equations:

$$\frac{\partial \Psi_e(\mathbf{u}^e)}{\partial \mathbf{u}^e} = \mathbf{l}^e\mathbf{u}^e - \mathbf{f}^e = 0 \tag{6a}$$

$$\mathbf{u}^e = \mathbf{l}^{e-1}\mathbf{f}^e \tag{6b}$$

To apply the method to an entire mesh, a standard assembly procedure is used. The local matrices $\mathbf{l}^e$ and vectors $\mathbf{f}^e$ are assembled to form the global matrix $\mathbf{L}$ and the global vector $\mathbf{F}$, respectively. The global nodal degrees of freedom $\mathbf{U}$ are thus obtained as:

$$\mathbf{U} = \mathbf{L}^{-1}\mathbf{F} \tag{7}$$

The penalisation strategy embedded in Eq. (4) makes the method suitable even for configurations with sparse sensor coverage, i.e., for elements lacking direct strain measurement data. However, previous studies [15,16] have shown that while the method maintains reasonable accuracy for moderately sparse configurations, it achieves higher accuracy when the structure is equipped with a dense network of strain sensors.

3. Strain pre-extrapolation methods

In the previous section, the importance of the availability of strain information for the iFEM was highlighted. In this section, two strain pre-extrapolation methods which can be used to feed iFEM with extrapolated strain components from a limited number of physical sensors are described in detail, focusing on their formulation, strength, and limitations.

3.1. Smoothing Element Analysis

The Smoothing Element Analysis (SEA) is an FE-based strain/stress extrapolation technique introduced by Tessler et al. in [35]. Although it has been used for both strain and stress extrapolation, in the context of this work, only the application to strain is considered; however, the same formulation can be adopted for stress as well. The method is based on the discretisation of the structural domain with Finite Elements and on the consequent expression of the strain field in terms of unknown nodal degrees of freedom and known shape functions. The nodal degrees of freedom for an SEA element are illustrated in Fig. 1.

The first DOF, $\mathbf{s}$, represents the extrapolated strain value for each node. The remaining two, $\mathbf{s_x}$ and $\mathbf{s_y}$, are auxiliary DOFS used to enforce C^1 continuity in the extrapolated strain field, as discussed in the remainder of this paragraph. The strain field, $\varepsilon_{SEA}(x, y)$, is interpolated within the element using parabolic and linear shape functions:

$$\varepsilon_{SEA}(x, y) = \mathbf{P}\mathbf{s} + \mathbf{M}\mathbf{s_x} + \mathbf{L}\mathbf{s_y} \tag{8}$$

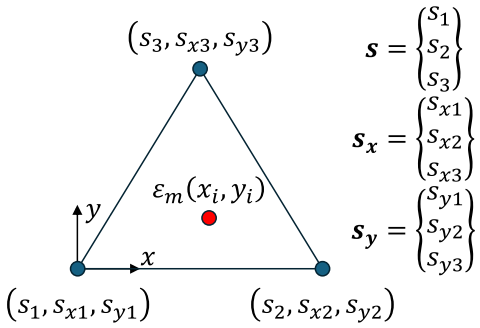

Fig. 1. SEA element.

whereas the auxiliary fields, d_x and d_y, are interpolated using linear shape functions:

$$\begin{aligned} d_x(x, y) &= \mathbf{P}\mathbf{s_x} \\ d_y(x, y) &= \mathbf{P}\mathbf{s_y} \end{aligned} \tag{9}$$

The linear shape functions $\mathbf{P} = [P_1(x, y), P_2(x, y), P_3(x, y)]$ are the area-parametric coordinates of the triangle, whereas $\mathbf{M} = [M_1(x, y), M_2(x, y), M_3(x, y)]$ and $\mathbf{L} = [L_1(x, y), L_2(x, y), L_3(x, y)]$ are the parabolic shape functions introduced in [45]. All these shape functions are C^0 continuous, and their explicit formulation can be found in [40]. To compute the unknown nodal values of the extrapolated strain field ($\varepsilon_{SEA}(x, y)$) that best fit the measured strain field, the method requires discrete measurements of deformation within the element ($\varepsilon_m(x_i, y_i)$), as shown in Fig. 1. The procedure is developed by minimising a functional representation of the error between the measured quantity and the analytical counterpart. In addition to this error, the functional includes additional terms to control the smoothness of the extrapolated field by controlling the continuity of the derivatives of the extrapolated function. The functional that expresses these conditions is:

$$\begin{aligned} \Phi^e = &\frac{1}{n^e}\sum_{i=1}^{n^e}\left[\left(\varepsilon_{SEA}(x_i, y_i)\right) - \varepsilon_m(x_i, y_i)\right)^2\right] \\ &+ \alpha\int_{A^e}\left[\left(\varepsilon_{SEA,x} - d_x\right)^2 + \left(\varepsilon_{SEA,y} - d_y\right)^2\right] dA^e \\ &+ \beta A^e\int_{A^e}\left[\left(d_{x,x}\right)^2 + \left(d_{y,y}\right)^2 + \frac{1}{2}\left(d_{x,y} + d_{y,x}\right)^2\right] dA^e \end{aligned} \tag{10}$$

where A^e is the area of the element, and n^e is the number of available strain measurements within the element.

The first term of the functional expresses the error between the extrapolated strain field and the measured one in n^e locations within the element.

The second term expresses the deviation of the derivatives of the extrapolated strain field ($\varepsilon_{SEA,x}$, $\varepsilon_{SEA,y}$) from the auxiliary fields of the SEA element (d_x, d_y). Since the auxiliary fields are C^0 continuous, when this term is minimised, $\varepsilon_{SEA,x} \to d_x$ and $\varepsilon_{SEA,y} \to d_y$. Therefore, $\varepsilon_{SEA,x}$ and $\varepsilon_{SEA,y}$ tend to a C^0 function and, hence, ε_{SEA} tends to a C^1 function. Through the weight α that multiplies this term, it is possible to set the enforcement level of the C^1 continuity of the extrapolated strain field, which is C^1 continuous for $\alpha \to \infty$.

The third term is a regularisation term involving the derivatives of the auxiliary fields. The term imposes a constraint on the strain curvatures controlled by the parameter β. This parameter should be set to a small value (compared to α) when the measured strains are perceived to be reasonably accurate and to a large value if the filtering of corrupted data is needed [35].

The minimisation of the functional concerning the nodal DOFs, $\mathbf{d^e} = [\mathbf{s}, \mathbf{s_x}, \mathbf{s_y}]^T$, leads to the formulation of a system of linear algebraic equa-

tions:

$$\frac{\partial \Phi^e}{\partial \mathbf{d^e}} \rightarrow \mathbf{K^e d^e} = \mathbf{f^e} \tag{11}$$

the expression of the $\mathbf{K^e}$ and $\mathbf{f^e}$ are:

$$\mathbf{K}^e = \frac{1}{n^e}\sum_{i=1}^{n^e} \mathbf{N}_i^T \mathbf{N}_i + \alpha \int_{A_e} \mathbf{B}_\alpha^T \mathbf{B}_\alpha \, dA^e + \beta A^e \int_{A_e} \mathbf{B}_\beta^T \mathbf{D} \mathbf{B}_\beta \, dA^e \tag{12}$$

$$\mathbf{f^e} = \frac{1}{n^e}\sum_{i=1}^{n^e} \varepsilon_m(x_i, y_i)\mathbf{N}_i^T \tag{13}$$

where:

$$\mathbf{N}_i = [\mathbf{P}(x_i, y_i), \mathbf{M}(x_i, y_i), \mathbf{L}(x_i, y_i)], \quad \mathbf{B}_\alpha = \begin{bmatrix} \mathbf{P}_{,x} & \mathbf{M}_{,x} - \mathbf{P} & \mathbf{L}_{,x} \\ \mathbf{P}_{,y} & \mathbf{M}_{,y} - \mathbf{P} & \mathbf{L}_{,y} - \mathbf{P} \end{bmatrix}$$

$$\mathbf{B}_\beta = \begin{bmatrix} \mathbf{0} & \mathbf{P}_{,x} & \mathbf{0} \\ \mathbf{0} & \mathbf{0} & \mathbf{P}_{,y} \\ \mathbf{0} & \mathbf{P}_{,y} & \mathbf{P}_{,x} \end{bmatrix}, \quad \mathbf{D} = \begin{bmatrix} 1 & \mathbf{0} & \mathbf{0} \\ \mathbf{0} & 1 & \mathbf{0} \\ \mathbf{0} & \mathbf{0} & 1/2 \end{bmatrix}, \quad \mathbf{0} = [0, 0, 0] \tag{14}$$

The classic assembly procedure of FE-based methods can extend the computation of matrices to a complex and multi-element mesh, thereby allowing the formulation of a global system of linear equations, $\mathbf{Kd} = \mathbf{f}$. The solution of this system leads to the computation of the nodal values of the extrapolated strain field that best fits the measured strain field at discrete locations, with the constraints and regularisation contributions induced by the terms multiplied by α and β. The SEA mesh used for the strain extrapolation can have elements that do not include any strain measurement. In this case, the first element of Eqs. (12) and (13) are set to 0.

The strength of SEA is represented by the possibility of extrapolating the strain field over geometrical domains that can be meshed with FE. Moreover, the method has a strong flexibility to different problems thanks to the parameters α and β, which can impose problem-specific conditions on the extrapolating functions. However, in some applications, this represents a limitation. In fact, the setting of these parameters requires some knowledge of the problem or a parametric study to find the best setting, thus sometimes resulting in an onerous and challenging process. The method is well-suited for extrapolating continuous fields in domains with no abrupt variations in strain. Consequently, it can be inaccurate when applied to built-up structures, where the complexity of the structure can lead to sudden variations in the strain field over the geometrical domain. In addition, for this kind of structure, another problem is the extrapolation of the strain field on parts of the structural domain that do not belong to the same surface of the measured strains, i.e. for a stiffened panel, strains measured on the skin can not be used to extrapolate strains on the stiffeners and vice versa. In addition, SEA extrapolates scalar quantities; consequently, SEA extrapolates each strain component at a time, and measured components can only be used to extrapolate the corresponding field. Another limitation of the approach is the mesh sensitivity of the method. The quality of the extrapolations depends on the SEA mesh adopted; therefore, a preliminary study of the extrapolating model is required.

The SEA approach described in this work is formulated for shell elements. However, a corresponding formulation for beam-like structures, based on a beam finite element, should also be feasible. To the authors' knowledge, such an extension has not yet been explored in previous studies, but it is expected to be straightforward and should not present significant difficulties, thereby making the method suitable for a wider range of geometrical domains.

3.2. Modal Virtual Sensor Expansion

The Modal Virtual Sensor Expansion (Modal VSE) has been recently coupled with iFEM in [41]. This method combines the features of the Modal Method, another shape sensing technique, with iFEM to overcome the limitations of these two techniques. Modal VSE is based on the extrapolation of strain measurements from a few sensors using the modal strain shapes of the structures.

In [46], O'Callahan et al. introduced the System Equivalent Reduction Expansion Process (SEREP), which can be used to virtually expand a small number of strain measurements into a larger set. A vector of S strain components, $(\boldsymbol{\varepsilon}_{VSE})_{S\times 1}$, can be divided into two subsets: S_m measured strains, $(\boldsymbol{\varepsilon}_m)_{S_m\times 1}$, and S_e expanded strains, $(\boldsymbol{\varepsilon}_e)_{S_e\times 1}$, such that $S = S_m + S_e$:

$$\boldsymbol{\varepsilon}_{VSE} = \begin{bmatrix} \boldsymbol{\varepsilon}_m \\ \boldsymbol{\varepsilon}_e \end{bmatrix} \tag{15}$$

If a FE discretisation of a structural domain is considered, the two vectors can be expressed through a modal expansion in terms of the vector of the modal coordinates, $\mathbf{q}$:

$$\boldsymbol{\varepsilon}_m = \boldsymbol{\Phi}_s^m \mathbf{q} \tag{16}$$

$$\boldsymbol{\varepsilon}_e = \boldsymbol{\Phi}_s^e \mathbf{q} \tag{17}$$

here, the modal matrices $(\boldsymbol{\Phi}_s^{(m,e)})_{S\times M}$ are constituted by M columns (the ith column being the set of strains corresponding to the ith mode shape of the FE model of the structure). By pseudo-inverting Eq. (16), we obtain:

$$\mathbf{q} = \left[(\boldsymbol{\Phi}_s^m)^T \boldsymbol{\Phi}_s^m\right]^{-1} (\boldsymbol{\Phi}_s^m)^T \boldsymbol{\varepsilon}_m \tag{18}$$

Substituting this into Eq. (17) provides:

$$\boldsymbol{\varepsilon}_e = \boldsymbol{\Phi}_s^e \left[(\boldsymbol{\Phi}_s^m)^T \boldsymbol{\Phi}_s^m\right]^{-1} (\boldsymbol{\Phi}_s^m)^T \boldsymbol{\varepsilon}_m \tag{19}$$

This equation allows the computation of the $\boldsymbol{\varepsilon}_e$ subset from the $\boldsymbol{\varepsilon}_m$ subset, enabling the reconstruction of the full strain set $\boldsymbol{\varepsilon}_{VSE}$ from the measured strains $\boldsymbol{\varepsilon}_m$. If $\boldsymbol{\varepsilon}_m$ corresponds to strains measured on a structure, Eq. (19) allows the expansion of these to strains at different locations or in different directions. Since the modal strain shapes are defined across the structural domain and for all strain components, this method is not restricted to extrapolating strain components within the same direction or surface, as seen in Smoothing Element Analysis (SEA). Instead, it can compute, for instance, strain components in the y-direction on a different surface, starting from discrete components in the x-direction.

For the method to be accurate, it is essential to select modes whose combination can represent the strain field that needs to be extrapolated. The selection of these modes defines the $\boldsymbol{\Phi}_s$ formulation. A criterion for the selection of the modes, based on the strain energy contribution of the single mode to the desired static deformed condition, has been adopted in [42,47] and can be applied here. The selection of the modes involves a preliminary study that is needed for the method. As for the parameters α and β described for SEA, this study requires some knowledge of the expected strain field. Furthermore, the number of modes (M) constrains the minimum number of measured strains, S_m, requiring that $S_m > M$.

Modal VSE exhibits some applicability advantages over SEA. However, it introduces a dependency on the knowledge of the structure's material properties, unlike standard iFEM, which only relies on strain-displacement relationships independent of material properties. Since Modal VSE requires the computation of modal characteristics dependent on these properties, its applicability is limited to cases where material properties are known, which is generally the case in engineering problems.

The Modal VSE requires the computation of the modal matrices $\boldsymbol{\Phi}_s^e$ and $\boldsymbol{\Phi}_s^m$; however, it is completely independent of the model used to obtain them. The modal characteristics can be extracted from beam, shell, or even solid FE models, as well as from analytical models or experimental tests, without compromising the generality of the method. This ensures that the approach remains adaptable to structures with widely varying geometries and suitable for a broad range of applications.

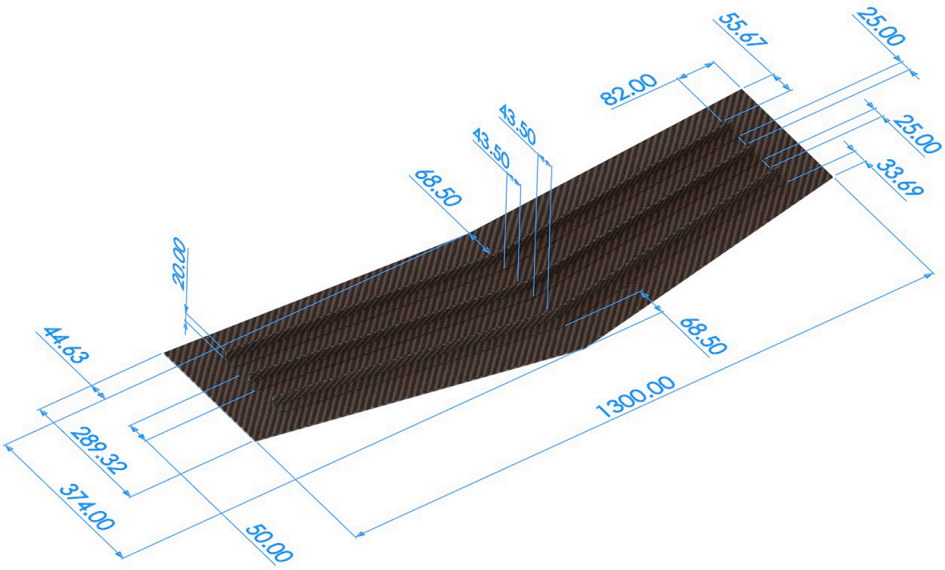

Fig. 2. Geometry of the test case [41]. All dimensions are expressed in mm.

Table 1
TWILL T-300 nominal properties.

$E_{11}[GPa]$	$E_{22}[GPa]$	ν_{12}	$G_{12}=G_{23}=G_{13}[GPa]$	Ply-thickness [mm]	$\rho[Kg/mm^3]$
59.7	59.7	0.09	3.8	0.25	1.5E-06

4. Numerical comparison

This section compares SEA and Modal VSE numerically on the strain pre-extrapolation of a composite wing-shaped stiffened panel. The comparison is first evaluated based on the extrapolation of the strain from a small set of measured sensors. Then, the extrapolated set of sensors is fed into the iFEM, and the accuracy of the shape sensing is also assessed.

4.1. Test case

The analysed numerical test case is a composite wing-shaped stiffened panel, whose geometrical parameters are presented in Fig. 2. The flat part of the panel is constituted of a laminate whose stacking sequence is $[45/0/0/45/0/0/0/45]_s$. The three T-section stiffeners have the exact same lamination on the web, whereas the stacking sequence of the two caps is obtained by folding the webs' lamination by ninety degrees. All the layers of the composite are made of a TWILL T-300 carbon-fibre fabric prepreg. The characteristics of the prepreg are reported in Table 1.

Three FE models of this structure have been developed. The first one, the iFEM model, is constituted of 960 iQS4 quadrilateral elements [43], 1035 nodes, and is shown in Fig. 3. This model is the one used for the application of iFEM. From this model, a high-fidelity model, the direct model, is obtained by splitting each quad element into four elements, thus generating a refined mesh of 3840 NASTRAN CQUAD4 elements. This second model is used to simulate the testing condition of the structure and to generate the reference strains and displacements adopted to evaluate the accuracy of the strain pre-extrapolations and shape sensing. Moreover, this model is also used to compute the modal characteristics of the structure for the use of the Modal VSE. Two other models are generated for the application of SEA to the structure. These models, composed of triangular elements, will be described in the following paragraph.

The boundary conditions considered for this study are simple supports at the tips of the two half-wings (Fig. 4). The panel is loaded with

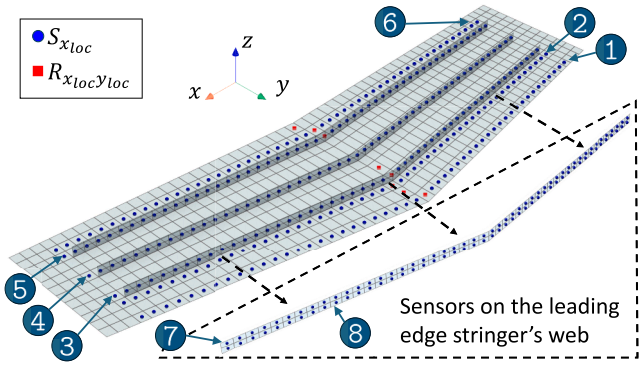

Fig. 3. iFEM model including the strain sensors of the optimised configuration.

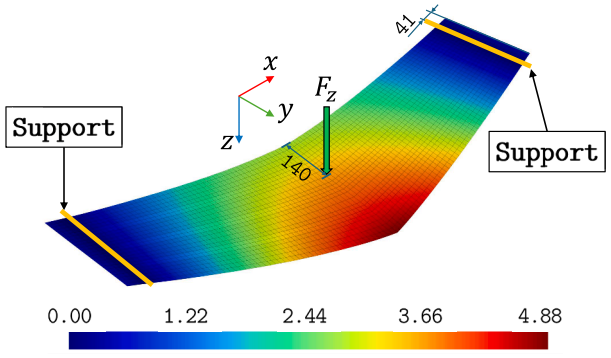

Fig. 4. Boundary conditions and target deformed shape of the test case. All dimension are expressed in mm.

a concentrated force, $F_z = 200N$, applied at the root of the wing. The location of the concentrated force along the chord length is designed to generate a complex bending and torsion deformation on the wing. Under this loading condition, the displacement field resulting from the analysis of the direct model is reported in Fig. 4.

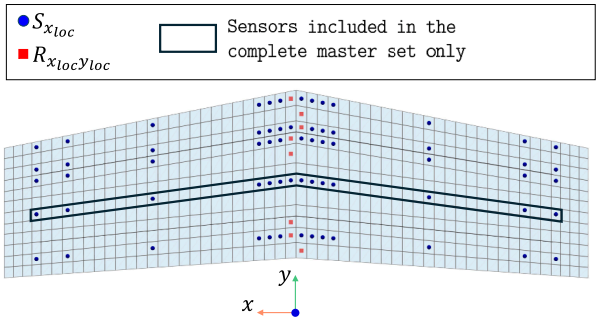

Fig. 5. Master sets of sensors on the panel. The Complete master set includes all the sensors represented in the figure, whereas the Reduced master set does not include the sensors within the black perimeter.

4.2. Sensor configuration

The application of the strain pe-extrapolation requires the definition of two families of sensors. The actually measured set of sensors will be referred to as the master set. The master set, plus the strain extrapolated with the methods object of this work, will be defined as the expanded set. For this study, two master sets and one expanded set are considered.

The set of sensors, shown in Fig. 3, is an optimised sensor configuration for the application of iFEM. The configuration was derived in [48] through an optimisation process carried out with a Genetic Algorithm. As a consequence, the configuration guarantees high accuracy for shape sensing. The configuration includes eight lines of sensorised elements with sensors measuring the strain along the respective line's direction (x-loc). Moreover, eight strain rosettes are also considered in the configuration. Although this configuration ensures extremely accurate shape sensing, it involves a considerable number of sensors. For this reason, the objective of the present study is to reproduce the same level of strain information as the optimised configuration by expanding the strain field from a reduced subset of master sensors, thereby decreasing the number of physical sensors that must be installed without compromising shape-sensing performance. To achieve that, two master sets are tested. The first one considers a subset of sensors from 5 out of the eight measuring lines of the optimised configuration. This configuration sufficiently covers the geometrical domain of the panel. This master set will be defined as Complete master set and includes all the sensors presented in Fig. 5. The sensors included in this set represent 18% of the sensors included in the optimised set. On the other hand, a reduced set of master sensors is considered to evaluate the adaptability of the extrapolation methods to more sparse sensor configurations. This second configuration considers a broad area of the structure without physical sensors, where the strains are nonetheless extrapolated. This configuration is defined as Reduced master set and is obtained by removing the sensors enclosed in the back square of Fig. 5. This set of sensors represents 15% of those included in the optimised set. These master sets are not used indiscriminately for SEA and Modal VSE. In fact, the two methods have different characteristics that adapt to different master sensor configurations. For this reason, the sets of sensors will be slightly modified to suit the requirements of each method. A detailed description of the master sets for each method is provided in the following sections.

All the sensor configurations illustrated in this paragraph are intended in a back-to-back configuration, i.e. sensors are placed on both the external surfaces of the plate at the designed locations.

4.3. SEA setup

The application of SEA requires the definition of a SEA model. For this application, two models are considered to evaluate the mesh's influence on the accuracy of SEA. Both SEA models are obtained by splitting the quad element of the iFEM model into four triangular elements, according to the pattern shown in Fig. 6. This pattern has proven optimal for using SEA in several applications [37,40,45].

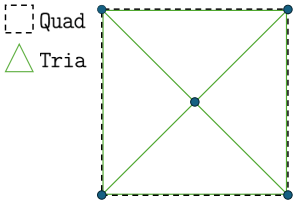

Fig. 6. Splitting pattern for the extraction of the SEA mesh from the iFEM mesh.

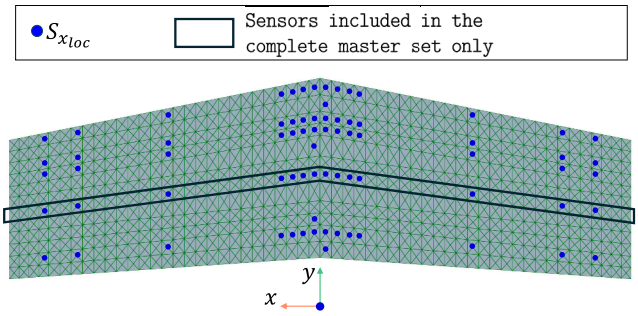

Fig. 7. Undivided SEA mesh - This model discretises the skin panel using a single mesh.

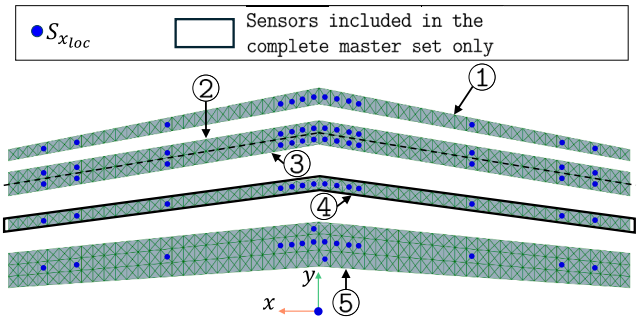

Fig. 8. Zones SEA mesh - This model discretises the skin panel using five separate meshes.

The first SEA mesh, labelled as Undivided SEA mesh, considers the whole panel as a unique mesh (Fig. 7). In this case, the master sensors are simultaneously used to expand the strains to the optimised sensor configuration in a single extrapolation process for the entire skin of the panel.

The second model, labelled as Zones SEA mesh, is obtained from the previous one by dividing the mesh into five zones, as illustrated in Fig. 8. For this case, each zone is treated separately, and the strains are extrapolated within each zone, considering only the master sensors located within the zone itself. This second model is designed to smooth possible sharp variations of the strain components between the sensing lines.

The SEA applicability to the extrapolation of scalar values required the modelisation of the panel and the stringer separately since the extrapolated strains on the two parts have a completely different direction, and information on the strain field on one component can not be used for extrapolating strains on the other component. Consequently, the SEA process is applied to the two parts separately. This limitation also requires physical sensors to be applied to both parts of the structure. For this reason, in addition to the sensor master sets described in Fig. 5, the master sets used for SEA include the additional sensors on the leading edge's stringer shown in Fig. 9. The scalar extrapolation nature of SEA also prevents the use of all three strain components from the rosettes for the extrapolation of the strains along the x-loc direction. Therefore, the

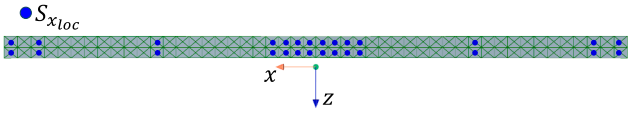

Fig. 9. Additional master sensors on the leading edge stringer for the application of SEA.

Table 2
Results of the parametric study for the application of SEA. The table shows the influence of the α parameter and the selected kind of mesh for the extrapolation process.

	Undivided SEA mesh	Zones SEA mesh
α	$RMSE$ [$\mu\varepsilon$]	$RMSE$ [$\mu\varepsilon$]
10^{-5}	7.8	8.9
10^{-4}	8.3	9.5
10^{-3}	8.3	9.5
10^{-2}	8.3	9.5
10^{-1}	8.3	9.5
10^{0}	8.3	9.5
10^{1}	8.4	9.6
10^{2}	8.9	9.7
10^{3}	12.3	10.3
10^{4}	13.8	11.9

rosettes represented in Fig. 5 are only used as mono-axial strain gauges along the x-loc direction for the SEA process, as highlighted in Figs. 7, 8.

The application of SEA also requires the setting of the method's parameters. Therefore, the first step for this method is studying the influences of the parameter α and of the SEA mesh. On the other hand, the β parameter is fixed and set to a small value ($\beta = 10^{-6}$), as prescribed in the case where there is good confidence in the accuracy of the measured strains [40,49]. To assess the influence of α, the parameter varies from 10^{-5} to 10^{4} with a step of 10. For each value, the extrapolation of the strains is performed using the Complete master set on both the Undivided SEA mesh and the Zones SEA mesh to evaluate the performance of the two different discretisations. For each strain pre-extrapolation, the RMSE is computed for all the n strain components measured with the sensors of the optimised configuration:

$$RMSE = \sqrt{\frac{1}{n}\sum_{i=1}^{n}(\varepsilon_i^m - \varepsilon_i)^2} \tag{20}$$

In eq. 20, ε_i^m represents the reference strain value extracted from the high fidelity direct model and ε_i represents the same strain value from the extrapolated set of strains. The extrapolated set of strains also includes the reference value of the strains from the master set.

The results of this parametric study are summarised in Table 2. The results show that SEA is robust to variations in α within the range $[10^{-5}, 10^{0}]$. In fact, for values within this range, the $RMSE$ does not show significant fluctuations. However, the minimum value of the $RMSE$ is obtained for $\alpha = 10^{-5}$ for both the considered SEA meshes. The influence of the mesh type does not have a considerable impact on the error. Nevertheless, the Undivided SEA mesh consistently shows higher accuracy for small values of α. In conclusion, the configuration that considers the Undivided SEA mesh with $\alpha = 10^{-5}$ is the one showing the highest accuracy, and is the one that will be considered in the comparison study against the Modal VSE.

4.4. Modal VSE setup

For the application of the Modal VSE, the master sets of sensors and the optimised expanded set are precisely the ones in Fig. 5 and 3, respectively. Thanks to its higher flexibility, the Modal VSE can utilise sensors only on the panel to extrapolate the strain field on the stringer's web, thus eliminating the need for additional sensors on this component. Moreover, all three components of the strain rosettes can be used since the method is able to expand the strains to different components than the one measured. The Modal VSE pre-extrapolation technique requires setting fewer parameters with respect to SEA and is mesh-independent. However, it necessitates computing the structure's modal strain shapes and selecting the modes most relevant to the strain field that needs to be extrapolated. To do that, a technique based on computing the potential strain energy contribution of each mode to a target deformed shape of the structure has been formulated in [42]. Although this technique requires knowledge of the target deformed shape, the selection of modes with this criterion has proven to be robust to variations in the load case [41]. For the current application, the first 40 modes of the structure have been computed. Out of these 40 modes, the first 18 modes account for 98.4% of the total strain deformation energy of the target deformed shape (Fig. 4), and therefore they are selected for the application of the Modal VSE.

Table 3
Results of the comparison between SEA and Modal VSE in terms of $RMSE$.

	Complete master set		Reduced master set	
	SEA	Modal VSE	SEA	Modal VSE
$RMSE$ [$\mu\varepsilon$]	7.8	4.3	9.2	4.2

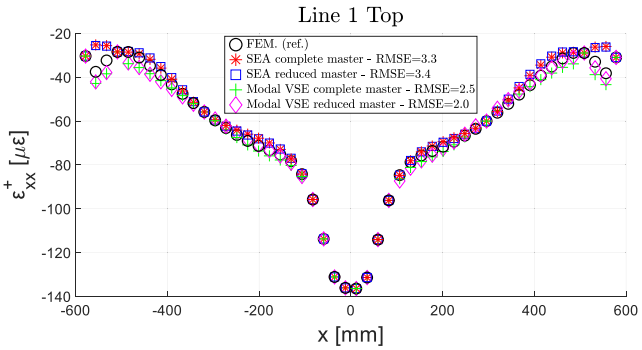

Fig. 10. Strain pre-extrapolation results for Line 1 on the flat side (Top) of the panel.

4.5. Strain pre-extrapolation comparison

In this section, a comparison is performed in terms of strain pre-extrapolation for SEA and Modal VSE.

In Table 3, the $RMSE$ obtained for the Modal VSE and SEA for the two considered master sets of measured sensors are summarised. The $RMSE$ are computed over all the strain components included in the optimised configuration of sensors. The results show that the Modal VSE is more accurate than SEA for both sets of master sensors. Moreover, the analysis proves that Modal VSE is robust to the reduction of provided strain information. In fact, the $RMSE$ is equal to 4 $\mu\varepsilon$ independently of the considered master set. On the contrary, the SEA shows a slight decrease in accuracy and a consequent increase in the $RMSE$ from 8 $\mu\varepsilon$ to 9 $\mu\varepsilon$ when the measured sensors are reduced.

A more detailed comparison can be achieved by analysing the trend of the extrapolated strains along the eight sensing lines of the optimised configuration (Fig. 3). The entire set of extrapolated strains is reported in Appendix A. In this section, only the more critical lines for comparing SEA and Modal VSE are reported and commented. The extrapolated strains and the reference ones for Line 1 are shown in Fig. 10.

For this case, the reported strains are relative to the panel's flat surface (Top). For this sensing line, several sensors are included in the mas-

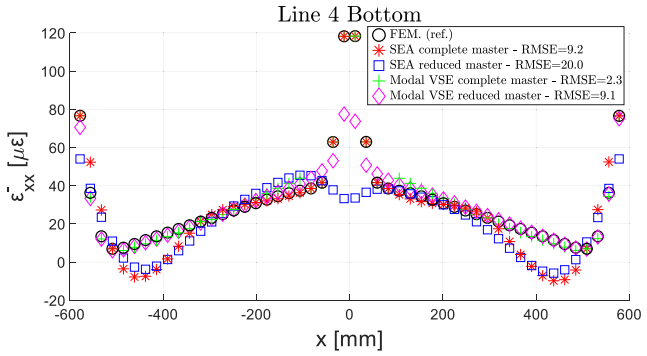

Fig. 11. Strain pre-extrapolation results for Line 4 on the stiffened side (Bottom) of the panel.

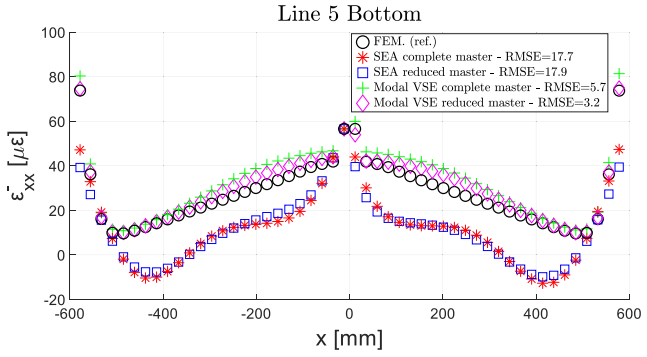

Fig. 12. Strain pre-extrapolation results for Line 5 on the stiffened side (Bottom) of the panel.

ter sets, and both the Modal VSE and SEA can accurately reconstruct the strain along the line.

On the other hand, Fig. 11 shows the trend of the strain extrapolation for Line 4 on the stiffened surface of the panel (Bottom). Sensing line number 4 is the one that includes physical sensors only in the complete master set. The analysis of the trends shows that SEA, even when the complete master set is considered, struggles to reproduce the real strain distribution. Moreover, when the master set of sensors is reduced and does not include sensors on Line 4, the RMSE for SEA increases rapidly. On the contrary, the Modal VSE shows a higher level of robustness. In fact, although the accuracy decreases for the reduced master set, the method can replicate the strain distribution, even when no strain information is acquired on Line 4. The RMSE for Modal VSE is consistently lower than that for SEA for every considered master set. This phenomenon highlights the impressive capability of extrapolation of the Modal VSE, even for regions of the domain where strain information is poor or absent.

The same behaviour can be observed for Line 5 in Fig. 12. Only one strain sensor that belongs to Line 5 is included in both the master sets. However, this sensing line is close to Line 6, where several physical sensors are included in the master sets. The proximity of this strain information does not help SEA to obtain reasonable extrapolations, whereas the Modal VSE, also in this case, performs strongly better than SEA.

Finally, another sensing line worth analysing is Line 7. This line lies on the front stringer of the panel. It is essential to note that for the extrapolation of strains on this line, SEA includes the master sensors in Fig. 9, whereas the Modal VSE does not consider any master sensor on the line. Once again, the extrapolation results in Fig. 13 show that the Modal VSE can extrapolate the strains in portions of the structure not sensorised with any physical sensors, with an accuracy higher than that reached by SEA fed with more strain information.

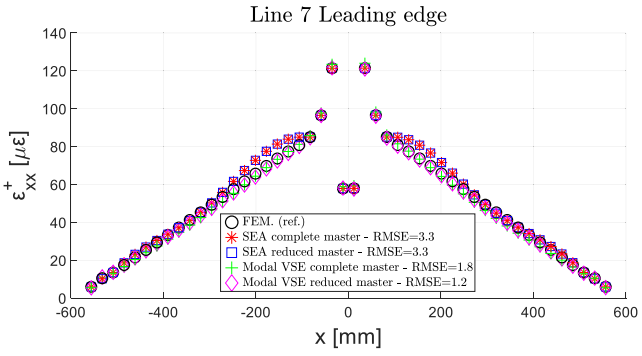

Fig. 13. Strain pre-extrapolation results for Line 7 on the face of the stringer towards the leading edge (Leading edge).

4.6. Shape sensing comparison

In this section, the pre-extrapolated strains are used as input to perform shape sensing with iFEM. Specifically, to compare the features of SEA and the Modal VSE and highlight their characteristics, the best-performing configurations are considered for each method. Therefore, the strain pre-extrapolation with SEA is performed using the complete master set of sensors with $\alpha = 10^{-5}$ and the undivided SEA mesh. In contrast, the reduced master set of sensors is used for the Modal VSE. Starting from their respective master sets of measured sensors, both methods are used to extrapolate the strains to the whole optimised configuration of sensors, which is then used to perform iFEM. The accuracy of the iFEM is evaluated through three percentage-based errors and two absolute errors concerning the reconstructed transverse displacements, w (along z direction), relative to the target deformed shape in Fig. 4:

- The percentage root mean squared error of the transverse displacements over the 1035 nodes of the inverse mesh:

$$\%RMSE_w = 100 \times \sqrt{\frac{1}{1035}\sum_{i=1}^{1035}\left(\frac{w_i - w_i^{ref}}{w_{max}^{ref}}\right)^2} \tag{21}$$

  where w_i are the reconstructed transverse displacements, w_i^{ref} are the reference transverse displacements, computed from the analysis of the direct mesh, and $w_{\max}^{ref}$ is the maximum value of the reference transverse displacements. This error, computed over the whole structure, measures the global accuracy of the shape reconstruction.
- The percentage error on the ith node:

$$\%Ew_i = 100 \times \left(\frac{|w_i - w_i^{ref}|}{|w_{max}^{ref}|}\right) \tag{22}$$

- The percentage error computed in the node where the maximum reference transverse displacement is experienced:

$$\%Ew_{max} = 100 \times \left(\frac{|w_{max} - w_{max}^{ref}|}{|w_{max}^{ref}|}\right) \tag{23}$$

  This error is a punctual one, allowing for the measurement of the reconstruction's accuracy in the most significant displacement.
- The root mean squared error of the transverse displacements over the 1035 nodes of the inverse mesh:

$$RMSE_w = \sqrt{\frac{1}{1035}\sum_{i=1}^{1035}\left(w_i - w_i^{ref}\right)^2} \tag{24}$$

- The absolute error computed in the node where the maximum reference transverse displacement is experienced:

$$Ew_{max} = |w_{max} - w_{max}^{ref}| \tag{25}$$

The results of the shape sensing in terms of $\%Erms_w$, $\%Ew_{\max}$, $RMSE_w$, and $Ew_{\max}$ are reported in Table 4, whereas the distributions of $\%Ew_i$ are reported in Figs. 14 and 15. In Table 4, the results of the

Table 4
Results of the shape sensing in terms of $\%Erms_w$, $\%Ew_{\max}$, $RMSE_w$, and $Ew_{\max}$.

	SEA + iFEM	Modal VSE + iFEM	Nominal strains + iFEM
$\%RMSE_w$	2.95	0.97	1.05
$\%Ew_{\max}$	3.65	1.96	4.02
$RMSE_w$ $[mm]$	0.14	0.047	0.051
$Ew_{\max}$ $[mm]$	0.18	0.096	0.20

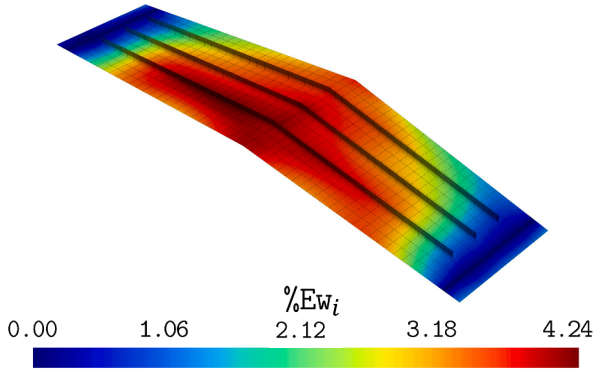

Fig. 14. $\%Ew_i$ distribution for the shape sensing performed with SEA coupled with iFEM.

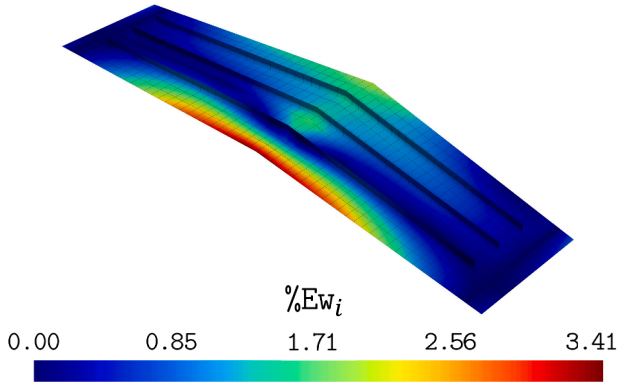

Fig. 15. $\%Ew_i$ distribution for the shape sensing performed with Modal VSE coupled with iFEM.

shape sensing, where all nominal strains of the optimised sensor configuration are used, without any pre-extrapolation, are also reported for comparison.

The results show that iFEM is an exceptionally stable shape sensing method when processing input strains affected by inaccuracy. For every considered configuration, the errors never exceed 5%, proving that both the strain pre-extrapolation methods can lead to precise shape sensing. However, upon closer examination of the error parameters, the Modal VSE coupled with iFEM demonstrates higher accuracy. The global accuracy, measured by the $\%Erms_w$ parameter, tends to the one obtained with the nominal strain values, with a value of 0.97%, which is significantly lower than that obtained with SEA. Moreover, the $\%Ew_{\max}$ is also lower for Modal VSE ($\%Ew_{\max} = 1.96$) than for SEA ($\%Ew_{\max} = 3.65$). The distributions of $\%Ew_i$ in Figs. 14 and 15 confirm these results. The deflections reconstructed with SEA coupled with iFEM show a uniform distribution of the error over the panel, with a broad area where the error is close to 4%. In contrast, the shape sensing with the help of the Modal VSE shows a local rise in the error only in a small portion of the panel at the trailing edge, where the error reaches 3.4%. In the remaining portions of the structure, the error is comprised between 0% and 1.7%. It is worth noting that the higher accuracy shown by the Modal VSE is obtained with a master set of measured sensors that includes fewer sensors than that of SEA, and does not include sensors on the stringer.

The shape sensing analysis reveals that, although both models yield adequate accuracy, the Modal VSE produces more reliable displacement reconstructions with iFEM. These results are obtained using deterministic values of the input strains, which are derived from a finite element model of the test case. Moreover, the errors in Table 4 highlight an unexpected behaviour. In most cases, the pre-extrapolation leads to smaller errors than the iFEM fed with the nominal strains. This phenomenon can be explained by the effect that perturbed inputs can have on iFEM. As reported in the uncertainty propagation study in [16], strain inputs affected by small errors, as in the case of the discrepancies introduced by the pre-extrapolation, can statistically produce both slightly better and worse shape sensing accuracy, in the neighbourhood of the unperturbed result. In this case, the beneficial coincidence is revealed. Therefore, to consider different scenarios that may not lead to this favourable condition and to test the robustness of the methods to the variability of the strains, it is necessary to perform an uncertainty propagation analysis. This analysis is presented in the next section.

5. Uncertainty propagation analysis

An uncertainty propagation analysis is performed in this section to better understand the behaviour of SEA and Modal VSE in real scenarios, where sensors are affected by noise and uncertainties from different sources. The process of uncertainty quantification involves analysing the probability density function (PDF) of the output and its statistical moments when the model inputs are subject to variability. A commonly adopted approach for this type of analysis is the Monte Carlo Simulation (MCS). In this method, each input variable is assigned a probability distribution. Multiple samples are then drawn from these distributions to generate a variety of input combinations for the model under study. These sampled inputs are used to run the model repeatedly–in this context, the sensor extrapolations and the consequent shape sensing algorithms, resulting in a statistical description (PDF) of the output. The accuracy of the resulting PDF depends on the number of input combinations generated. When using basic random sampling, a large number of simulations is typically needed, which leads to high computational cost. Alternative sampling strategies can improve simulation efficiency and accuracy by using fewer input samples. One such technique is Latin Hypercube Sampling (LHS), a stratified sampling method that ensures all regions of each variable's distribution are adequately represented [50]. This leads to more accurate results even with a reduced number of samples.

To take into account the deviation from the deterministic values present in experimental strain measurements, a normally distributed error with zero mean and a standard deviation of 10% of the nominal value is added to the strain values obtained from the deterministic FEM numerical analysis. For this analysis, the number of samples extracted with LHS is 1000.

The strains affected by the sampled errors are used to perform strain pre-extrapolation with SEA and Modal VSE. Replicating the process described in the previous sections, the extrapolated strains are then used to perform shape sensing with iFEM. The configurations, in terms of master sets and expanded sets of sensors, are the same as those adopted in Section 4.6.

The resulting PDFs of the $RMSE$ (Eq. 20) for the extrapolated strains, $\%RMSE_w$ (Eq. 24), and $\%Ew_{\max}$ (Eq. 25) for the reconstructed displacements are reported in Figs. 16, 17, and 18, respectively.

Fig. 16 allows for evaluating the effect of uncertainty on the strain pre-extrapolation capabilities of the methods selected for this comparison work. The PDF relative to the Modal VSE shows a mean value (μ) that is 1.7 times smaller than the one experienced by SEA. Moreover, the standard deviations (σ) of the two PDFs are comparable, with Modal VSE showing a slightly higher value and, consequently, a somewhat higher variability of the RMSE in consequence of uncertainties in the strains. The same trend can be inferred from the Coefficient of Variation (CoV) reported in the graphs. It is essential to highlight that the Modal

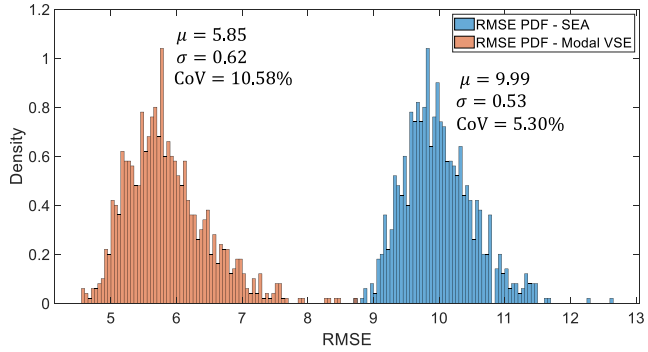

Fig. 16. PDF of the $RMSE$ for the extrapolated strains, when the master sensors are affected by 10% normally distributed error.

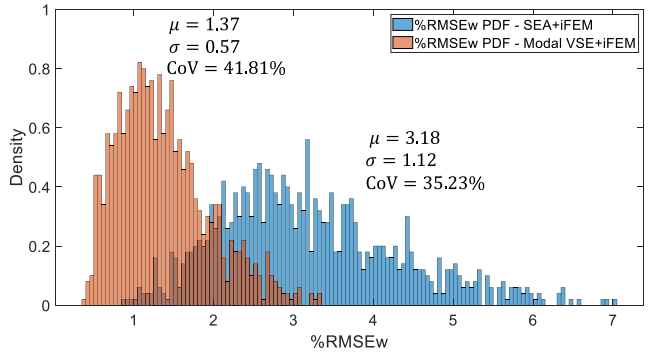

Fig. 17. PDF of the $\%RMSE_w$ for reconstructed displacements, when the master sensors are affected by 10% normally distributed error.

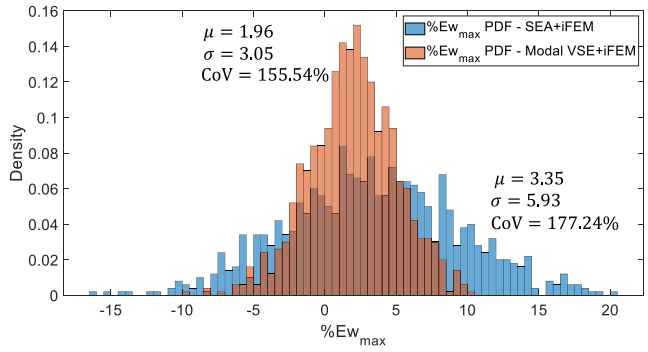

Fig. 18. PDF of the $\%Ew_{\max}$ for reconstructed displacements, when the master sensors are affected by 10% normally distributed error.

VSE's PDF is almost entirely on the left of the SEA's one. Therefore, the strain pre-extrapolations that are more affected by errors performed with Modal VSE are more accurate than the best ones performed with SEA.

The analysis of Figs. 17 and 18 lead to evaluations of the robustness of the two methods when used to feed iFEM for shape sensing. In Fig. 17, the PDFs of $\%RMSE_w$, which measures the global accuracy of the shape sensing, are presented for the two methods. The coupling of Modal VSE with iFEM shows more robust results in terms of mean value and standard deviation. In this case, the two distributions partially overlap in the $\%RMSE_w$ range between approximately 1.5% and 3%, although the overlap occurs in a region of relatively low probability density for both models. Fig. 18 shows the PDFs of the error on the maximum deflection. The comparison of the two models on this parameter is less straightforward. Modal VSE and SEA both show a higher variability, highlighted by the significant value of σ and CoV. Moreover, the PDFs overlap in a broad range of $\%Ew_{\max}$ values. However, also in this case, the mean value of the error for the Modal VSE is lower than that experienced by SEA. The same trend occurs for the standard deviations.

To summarise, the uncertainty in strain measurements consistently has a more negative effect on SEA than on Modal VSE. The Modal VSE yields more accurate and robust results in both the strain pre-extrapolation process and shape sensing when coupled with iFEM. Additionally, this behaviour is observed when the Modal VSE utilises a smaller number of actually measured strain sensors, with no strain information available on the stringer of the structure.

6. Conclusions

This work presents a comparative study between Modal VSE and SEA, two strain pre-extrapolation methods used to expand sparse strain measurements so that the strain-based shape-sensing algorithm iFEM can be provided with sufficient input data. Modal VSE is a recently formulated method that has shown promising results, but still lacks rigorous benchmarking against well-established approaches such as SEA. The objective of this work is therefore to derive crucial insights, both in terms of accuracy and applicability, through such benchmarking, to guide researchers and industrial practitioners in selecting the most suitable tool for their specific application.

The comparison is numerically performed on a complex structure: a composite stiffened wing-shaped panel. This structure includes geometrical features typical of aerospace systems, posing challenging conditions for strain pre-extrapolation algorithms due to discontinuities in the strain field introduced by stiffeners and the overall geometric complexity of the built-up configuration. On this structure, Modal VSE demonstrates superior versatility and ease of use. The method is able to accurately reconstruct the strain field in several regions of the panel, including the stiffeners, even when only a limited number of physical sensors are installed on the skin. This leads to accurate displacement reconstruction with iFEM. Modal VSE also overcomes key limitations of SEA when applied to built-up structures. SEA performs well with smoothly varying strain fields but becomes impractical where abrupt strain variations occur. Moreover, SEA cannot extrapolate strains across different surfaces (i.e., from skin to stiffeners) or between different strain components, as it operates on scalar values independently. Modal VSE addresses these issues by relying on modal strain shapes, which are defined over the entire structural domain and for all strain components. From an application perspective, Modal VSE is also advantageous because SEA requires careful tuning of several parameters (α, β, SEA mesh), often necessitating a preliminary parametric study. The superior performance of Modal VSE is further supported by a study on the influence of input strain uncertainties, simulating experimental conditions.

Although Modal VSE offers greater versatility and accuracy, it introduces limitations for particular scenarios. When material properties are unknown or unreliable, SEA remains preferable. Modal VSE depends on computing the modal characteristics of the structure, which may be unfeasible or inaccurate if material characterization is poor. SEA, on the other hand, is completely independent of such information. Additionally, the combination of Modal VSE and iFEM is a recent development and is still only partially explored. Future work should investigate the potential of Modal VSE to further reduce sensor requirements. In the present study, although a consistent reduction in the number of physical sensors is achieved, the number of sensors required for extrapolation remains relatively high. Coupling Modal VSE with sensor optimization algorithms for the selection of the master set of physical sensors could overcome this limitation and represents a promising direction for future research.

CRediT authorship contribution statement

Marco Esposito: Writing – review & editing, Writing – original draft, Visualization, Validation, Software, Resources, Methodology, Investigation, Formal analysis, Data curation, Conceptualization.

Data availability

Data will be made available on request.

Declaration of competing interest

The authors declare that they have no known competing financial interests or personal relationships that could have appeared to influence the work reported in this paper.

Appendix A. Extrapolated strains

In this Appendix, the extrapolated strains from the numerical study are reported (Fig. A.1), along with the reference strains for all eight sensing lines of the optimised configuration (Fig. 3). The strains are reported for the flat side of the panel (Top), the stiffened side of the panel (Bottom), the face of the stringer towards the leading edge (Leading edge), and the surface of the stiffener towards the trailing edge (Trailing edge).

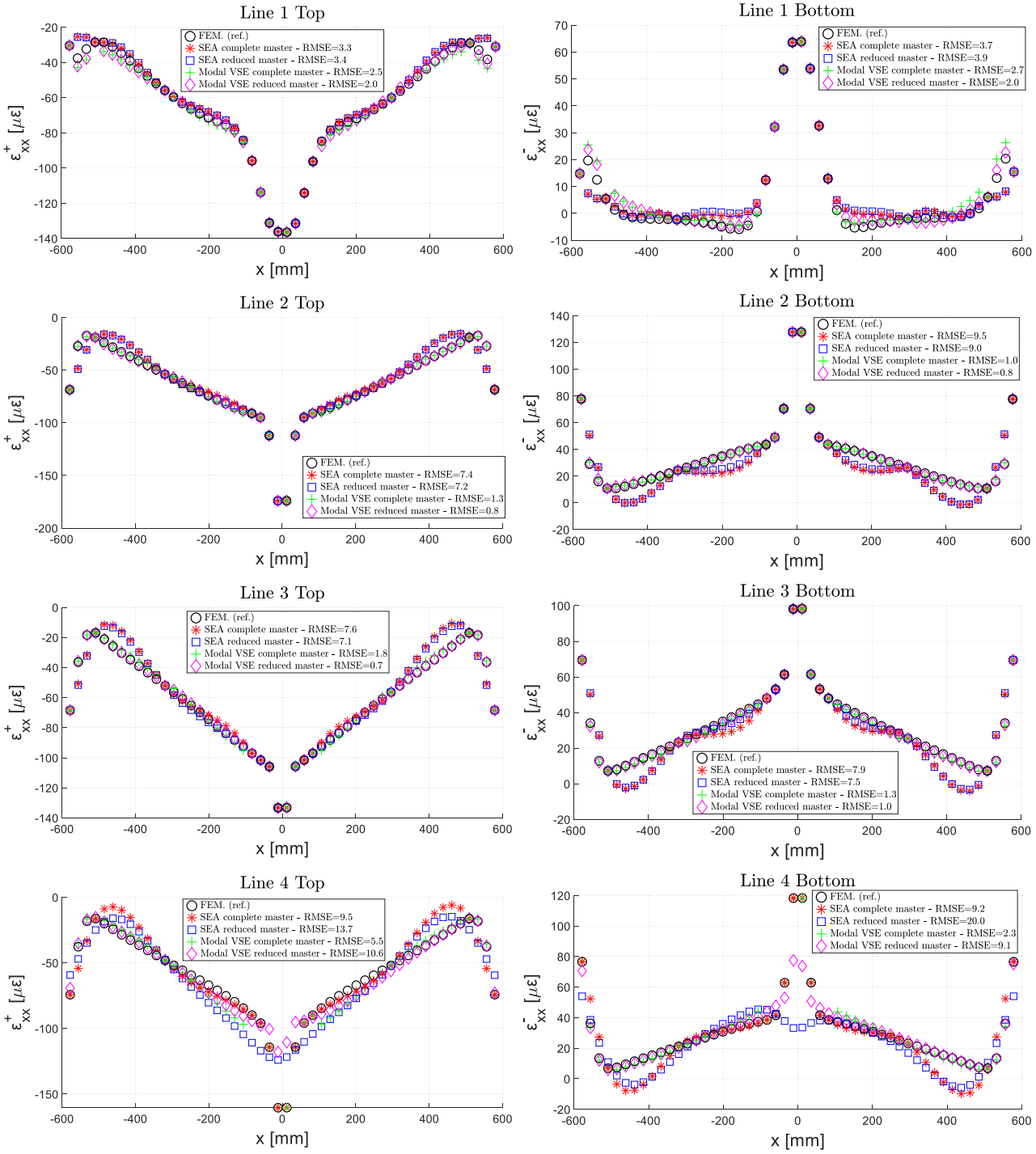

Fig. A.1. Extrapolated and reference strains for all eight sensing lines of the optimised configuration.

References

[1] L. Colombo, C. Sbarufatti, M. Giglio, Definition of a load adaptive baseline by inverse finite element method for structural damage identification, Mech. Syst. Signal Process. 120 (2019) 584–607. https://doi.org/10.1016/j.ymssp.2018.10.041

[2] R. Roy, M. Gherlone, C. Surace, A. Tessler, Full-Field strain reconstruction using uniaxial strain measurements: application to damage detection, Appl. Sci. 11 (4) (2021) 1681. https://doi.org/10.3390/app11041681

[3] M. Li, A. Kefal, B.C. Cerik, E. Oterkus, Dent damage identification in stiffened cylindrical structures using inverse finite element method, Ocean Eng. 198 (2020) 106944. https://doi.org/10.1016/j.oceaneng.2020.106944

[4] L. Colombo, D. Oboe, C. Sbarufatti, F. Cadini, S. Russo, M. Giglio, Shape sensing and damage identification with iFEM on a composite structure subjected to impact damage and non-trivial boundary conditions, Mech. Syst. Signal Process. 148 (2021) 107163. https://doi.org/10.1016/j.ymssp.2020.107163

[5] A. Airoldi, G. Sala, R. Evenblij, C. Koimtzoglou, T. Loutas, G.M. Carossa, P. Mastromauro, T. Kanakis, Load monitoring by means of optical fibres and strain gages, in: P.C. Wölcken, M. Papadopoulos (Eds.), Smart Intelligent Aircraft Structures (SARISTU), Springer International Publishing, Cham, 2016, pp. 433–469. https://doi.org/10.1007/978-3-319-22413-8_20

[6] T. Nakamura, H. Igawa, A. Kanda, Inverse identification of continuously distributed loads using strain data, Aerosp. Sci. Technol. 23 (1) (2012) 75–84. https://doi.org/10.1016/j.ast.2011.06.012

[7] M.J. Candon, M. Esposito, O. Levinski, N. Joseph, S. Koschel, R. Carrese, P. Marzocca, On the application of a long-short-term memory deep learning architecture for aircraft transonic buffet loads monitoring, in: AIAA Scitech 2020 Forum, 2020, https://doi.org/10.2514/6.2020-0702

[8] A. Kefal, C. Diyaroglu, M. Yildiz, E. Oterkus, Coupling of peridynamics and inverse finite element method for shape sensing and crack propagation monitoring of plate structures, Comput. Methods Appl. Mech. Eng. 391 (2022) 114520. https://doi.org/10.1016/j.cma.2021.114520

[9] S. Barbarino, O. Bilgen, R.M. Ajaj, M.I. Friswell, D.J. Inman, A review of morphing aircraft, J. Intell. Mater. Syst. Struct. 22 (9) (2011) 823–877. https://doi.org/10.1177/1045389X11414084

[10] T. de Souza Siqueira Versiani, F.J. Silvestre, A.B. Guimarães Neto, D.A. Rade, R.G. Annes da Silva, M.V. Donadon, R.M. Bertolin, G.C. Silva, Gust load alleviation in a flexible smart idealized wing, Aerosp. Sci. Technol. 86 (2019) 762–774. https://doi.org/10.1016/j.ast.2019.01.058

[11] V. Biscotti, R. Roy, M. Gherlone, Shape monitoring of morphing wing structures using the inverse finite element method, Comput. Struct. 309 (2025) 107652. https://doi.org/10.1016/j.compstruc.2025.107652

[12] R. Di Sante, Fibre optic sensors for structural health monitoring of aircraft composite structures: recent advances and applications, Sensors 15 (8) (2015) 18666–18713. https://doi.org/10.3390/s150818666

[13] H. Wang, P. Xiang, L. Jiang, Strain transfer theory of industrialized optical fiber-based sensors in civil engineering: a review on measurement accuracy, design and calibration, Sens. Actuators A 285 (2019) 414–426. https://doi.org/10.1016/j.sna.2018.11.019

[14] M. Gherlone, P. Cerracchio, M. Mattone, Shape sensing methods: review and experimental comparison on a wing-shaped plate, Prog. Aerosp. Sci. 99 (2018) 14–26. https://doi.org/10.1016/j.paerosci.2018.04.001

[15] M. Esposito, M. Gherlone, Composite wing box deformed-shape reconstruction based on measured strains: optimization and comparison of existing approaches, Aerosp. Sci. Technol. 99 (2020) 105758. https://doi.org/10.1016/j.ast.2020.105758

[16] M. Esposito, M. Gherlone, Material and strain sensing uncertainties quantification for the shape sensing of a composite wing box, Mech. Syst. Signal Process. 160 (2021) 107875. https://doi.org/10.1016/j.ymssp.2021.107875

[17] W.L. Ko, W.L. Richards, V.T. Fleischer, Applications of the Ko displacement theory to the deformed shape predictions of the doubly-tapered Ikhana wing, Report NASA/TP-2009-214652, NASA Dryden Flight Research Center; Edwards, CA, United States, 2009.

[18] H.-P. Wang, X.-S. Gong, X.-Z. Wang, S.-Y. Feng, T.-L. Yang, Y.-X. Guo, Discrete curvature-based shape configuration of composite pipes for local buckling detection based on fiber Bragg grating sensors, Measurement 188 (2022) 110603. https://doi.org/10.1016/j.measurement.2021.110603

[19] A. Tessler, J.L. Spangler, A Variational Principle for Reconstruction of Elastic Deformations in Shear Deformable Plates and Shells, Report NASA/TM-2003-212445, NASA Langley Research Center, Hampton, VA, United States, 2003.

[20] M. Gherlone, P. Cerracchio, M. Mattone, M.D. Sciuva, A. Tessler, An inverse finite element method for beam shape sensing: theoretical framework and experimental validation, Smart Mater. Struct. 23 (4) (2014) 045027. https://doi.org/10.1088/0964-1726/23/4/045027

[21] F. Zhao, L. Xu, H. Bao, J. Du, Shape sensing of variable cross-section beam using the inverse finite element method and isogeometric analysis, Measurement 158 (2020) 107656. https://doi.org/10.1016/j.measurement.2020.107656

[22] R. Roy, M. Gherlone, C. Surace, A shape sensing methodology for beams with generic cross-sections: application to airfoil beams, Aerosp. Sci. Technol. 110 (2021) 106484. https://doi.org/10.1016/j.ast.2020.106484

[23] U. Papa, S. Russo, A. Lamboglia, G.D. Core, G. Iannuzzo, Health structure monitoring for the design of an innovative UAS fixed wing through inverse finite element method (iFEM), Aerosp. Sci. Technol. 69 (2017) 439–448. https://doi.org/10.1016/j.ast.2017.07.005

[24] P. Cerracchio, M. Gherlone, A. Tessler, Real-time displacement monitoring of a composite stiffened panel subjected to mechanical and thermal loads, Meccanica 50 (2015) 2487–2496. https://doi.org/10.1007/s11012-015-0146-8

[25] F. Zhao, H. Bao, J. Liu, K. Li, Shape sensing of multilayered composite and sandwich beams based on refined zigzag theory and inverse finite element method, Compos. Struct. 261 (2021) 113321. https://doi.org/10.1016/j.compstruct.2020.113321

[26] A. Kefal, A. Tessler, E. Oterkus, An enhanced inverse finite element method for displacement and stress monitoring of multilayered composite and sandwich structures, Compos. Struct. 179 (2017) 514–540. https://doi.org/10.1016/j.compstruct.2017.07.078

[27] A. Kefal, I.E. Tabrizi, M. Tansan, E. Kisa, M. Yildiz, An experimental implementation of inverse finite element method for real-time shape and strain sensing of composite and sandwich structures, Compos. Struct. 258 (2021) 113431. https://doi.org/10.1016/j.compstruct.2020.113431

[28] A. Kefal, E. Oterkus, Isogeometric iFEM analysis of thin shell structures, Sensors 20 (9) (2020). https://doi.org/10.3390/s20092685

[29] E. Del Priore, L. Lampani, A methodology for applying isogeometric inverse finite element method to the shape sensing of stiffened thin-shell structures, Thin-Walled Struct. 199 (2024) 111837. https://doi.org/10.1016/j.tws.2024.111837

[30] M.Y. Belur, A. Kefal, M.A. Abdollahzadeh, S.D. Fassois, Damage diagnosis of plates and shells through modal parameters reconstruction using inverse finite-element method, Struct. Health Monit. 0 (0) (2024) https://doi.org/10.1177/14759217241249678

[31] F. Ganjdoust, A. Kefal, A. Tessler, A novel delamination damage detection strategy based on inverse finite element method for structural health monitoring of composite structures, Mech. Syst. Signal Process. 192 (2023) 110202. https://doi.org/10.1016/j.ymssp.2023.110202

[32] V. Biscotti, M. Esposito, M. Gherlone, A new single sensor based iFEM formulation for shape-sensing of thin-walled structures instrumented with single-sided sensor configurations: formulation, numerical assessment, and experimental validation, Mech. Syst. Signal Process. 232 (2025) 112700. https://doi.org/10.1016/j.ymssp.2025.112700

[33] J. Bardiani, C. Oppezzo, A. Manes, C. Sbarufatti, An inverse FEM for structural health monitoring of a containership: sensor network optimization for accurate displacement, strain, and internal force reconstruction, Sensors 25 (1) (2025). https://doi.org/10.3390/s25010276

[34] H.-P. Wang, C. Chen, Y.-Q. Ni, M. Jayawickrema, J. Epaarachchi, Computer-aided feature recognition of CFRP plates based on real-time strain fields reflected from FBG measured signals, Composit. Part B Eng. 263 (2023) 110866. https://doi.org/10.1016/j.compositesb.2023.110866

[35] A. Tessler, H.R. Riggs, C.E. Freese, G.M. Cook, An improved variational method for finite element stress recovery and a posteriori error estimation, Comput. Methods Appl. Mech. Eng. 155 (1) (1998) 15–30. https://doi.org/10.1016/S0045-7825(97)00135-7

[36] A. Kefal, I.E. Tabrizi, M. Yildiz, A. Tessler, A smoothed iFEM approach for efficient shape-sensing applications: numerical and experimental validation on composite structures, Mech. Syst. Signal Process. 152 (2021) 107486. https://doi.org/10.1016/j.ymssp.2020.107486

[37] R. Roy, A. Tessler, C. Surace, M. Gherlone, Efficient shape sensing of plate structures using the inverse finite element method aided by strain pre-extrapolation, Thin-Walled Struct. 180 (2022) 109798. https://doi.org/10.1016/j.tws.2022.109798

[38] E. Del Priore, L. Lampani, Shape sensing in plate structures through inverse finite element method enhanced by multi-objective genetic optimization of sensor placement and strain pre-extrapolation, Sensors 24 (2) (2024). https://doi.org/10.3390/s24020608

[39] M.A. Abdollahzadeh, I.E. Tabrizi, A. Kefal, M. Yildiz, A combined experimental/numerical study on deformation sensing of sandwich structures through inverse analysis of pre-extrapolated strain measurements, Measurement 185 (2021) 110031. https://doi.org/10.1016/j.measurement.2021.110031

[40] D. Oboe, L. Colombo, C. Sbarufatti, M. Giglio, Comparison of strain pre-extrapolation techniques for shape and strain sensing by iFEM of a composite plate subjected to compression buckling, Compos. Struct. 262 (2021) 113587. https://doi.org/10.1016/j.compstruct.2021.113587

[41] M. Esposito, A novel shape sensing approach based on the coupling of modal virtual sensor expansion and iFEM: numerical and experimental assessment on composite stiffened structures, Comput. Struct. 305 (2024) 107520. https://doi.org/10.1016/j.compstruc.2024.107520

[42] P. Bogert, E. Haugse, R. Gehrki, Structural shape identification from experimental strains using a modal transformation technique, in: 44th AIAA/ASME/ASCE/AHS/ASC Structures, Structural Dynamics, and Materials Conference, Norfolk, 2003. https://doi.org/10.2514/6.2003-1626

[43] A. Kefal, E. Oterkus, A. Tessler, J.L. Spangler, A quadrilateral inverse-shell element with drilling degrees of freedom for shape sensing and structural health monitoring, Eng. Sci. Technol. an Int. J. 19 (3) (2016) 1299–1313. https://doi.org/10.1016/j.jestch.2016.03.006

[44] A. Tessler, J.L. Spangler, A least-squares variational method for full-field reconstruction of elastic deformations in shear-deformable plates and shells, Comput. Methods Appl. Mech. Eng. 194 (2) (2005) 327–339. https://doi.org/10.1016/j.cma.2004.03.015

[45] A. Tessler, T.J.R. Hughes, A three-node mindlin plate element with improved transverse shear, Comput. Methods Appl. Mech. Eng. 50 (1) (1985) 71–101. https://doi.org/10.1016/0045-7825(85)90114-8

[46] J.C. O'Callahan, P. Avitabile, R. Riemer, System equivalent reduction expansion process, in: Proc. of the 7th Inter. Modal Analysis Conf., Las Vegas, 1989.

[47] M. Freydin, M.K. Rattner, D.E. Raveh, I. Kressel, R. Davidi, M. Tur, Fiber-optics-based aeroelastic shape sensing, AIAA J. 57 (12) (2019) 5094–5103. https://doi.org/10.2514/1.J057944

[48] M. Esposito, R. Roy, C. Surace, M. Gherlone, Hybrid shell-beam inverse finite element method for the shape sensing of stiffened thin-walled structures: formulation

and experimental validation on a composite wing-shaped panel, Sensors 23 (13) (2023). https://doi.org/10.3390/s23135962

[49] A. Tessler, Structural analysis methods for structural health management of future aerospace vehicles, in: Damage Assessment of Structures VII, 347 of *Key Engineering Materials*, Trans Tech Publications Ltd, 2007, pp. 57–66. https://www.scientific.net/KEM.347.57

[50] M.D. Mckay, R.J. Beckman, W.J. Conover, A comparison of three methods for selecting values of input variables in the analysis of output from a computer code, Technometrics 42 (1) (2000) 55–61. https://doi.org/10.1080/00401706.2000.10485979